

# A Cr-K emission line survey in young supernova remnants with *Chandra*

X.J. Yang<sup>1,2</sup>, H. Tsunemi<sup>3</sup>, F.J. Lu<sup>1</sup>, L. Chen<sup>2</sup>

## ABSTRACT

We performed a Cr-K emission line survey in young supernova remnants (SNRs) with the *Chandra* archival data. Our sample includes W49B, Cas A, Tycho and Kepler. We confirmed the existence of the Cr line in W49B and discovered this emission line in the other three SNRs. The line center energies, equivalent widths (EWs) and fluxes of the Cr lines are given. The Cr in Cas A is in a high ionization state while that in Tycho and Kepler is in a much lower one. We find a good positive correlation between Cr and Fe line center energies, suggesting a common origin of Cr and Fe in the nucleosynthesis, which is consistent with the theoretical predictions. We propose that the EW ratio between Cr and Fe can be used as a supplementary constraint on the progenitors' properties and the explosion mechanism.

*Subject headings:* ISM: supernova remnants – ISM: individual: W49B, Cas A, Tycho, Kepler

## 1. Introduction

The X-ray emission of young supernova remnants (SNRs) is predominantly from the ejecta heated by the reverse shock. Since the ejecta are metal abundant, their X-ray spectra usually show strong emission lines of heavy elements such as O, Ne, Mg, Si, S, Ar, Ca and

---

<sup>1</sup>Particle Astrophysics Center, Institute of High Energy Physics, Chinese Academy of Sciences, Beijing 100049, P.R. China, yangxj@mail.ihep.ac.cn, lufj@mail.ihep.ac.cn

<sup>2</sup>Department of Astronomy, Beijing Normal University, Beijing 100875, P.R. China

<sup>3</sup>Department of Earth and Space Science, Graduate School of Science, Osaka University, Toyonaka, Osaka 560-0043, Japan; tsunemi@ess.sci.osaka-u.ac.jp

Fe. Many works have focused on these emission lines from young SNRs, e.g. W49B (Hwang et al. 2000a; Miceli et al. 2006), Tycho (Tsunemi et al. 1986; Hwang et al. 1997), Cas A (Tsunemi et al. 1986; Holt et al. 1994; Hughes et al. 2000; Hwang et al. 2000b) and Kepler (Hatsukade et al. 1990; Kinugasa & Tsunemi, 1999; Cassam-Chenaï et al. 2004; Reynolds et al. 2007). Comparison of the abundance pattern of an SNR with the theoretical predictions could be used to constrain the properties of the corresponding supernova (SN) (e.g., Hughes et al. 1995; Rakowski et al. 2006).

For a long time the K lines from heavy elements such as Ti, Cr and Mn, which are expected to appear in 4–6 keV had not been detected in SNRs. The first and the only case, as far as we know, is the detection of the He-like lines of Cr and Mn in SNR W49B by the Advanced Satellite for Cosmology and Astrophysics (*ASCA*) (Hwang et al. 2000a) and *XMM-Newton* (Miceli et al. 2006). Hwang et al. (2000a) proposed that Cr, Mn and Ni would be the most promising heavy atomic species for future detection, since they are the most abundant elements next to Fe with K-shell emission lines at energies above  $\sim 4$  keV.

From nucleosynthesis theories (Woosley & Weaver 1994; Woosley & Weaver 1995; Thielemann et al. 1996) we know that Cr is mainly formed from the decay of Fe during SN explosions. SNRs from type Ia explosions are the top candidates for the detection of Cr emission, as the progenitors are completely destroyed during the SN explosions and all material is ejected into interstellar space. The Cr line emission could also be detected in a core-collapse SNR, if there is a large fraction of Cr formed outside the mass cut. In this paper, we report a Cr line survey in the young and bright SNRs W49B, Cas A, Tycho and Kepler using the abundant archival data collected by the *Chandra* X-ray observatory. We describe the observations and data analyses in § 2. The results are shown in § 3, discussion in § 4 and summary in § 5. All through this paper, the statistical uncertainties are given at 90% confidence level.

## 2. Observations and Data analyses

SNRs are important observational targets for *Chandra*. For example, as one of the largest projects, *Chandra* has observed the Cas A SNR for a few times with a total exposure time of 1 Ms (Hwang et al. 2004). The Kepler SNR was also observed for 750 ks (Reynolds et al. 2007). In this paper, we collected almost all the available *Chandra* ACIS-S data of the four SNRs. The detailed observation information is listed in Table 1. The data were processed using the CIAO software package (version 3.4). We created new level 2 event files for all the observations we used, applying gain map, time-dependent gain and charge transfer inefficiency corrections with the latest released calibration files (CALDB version 3.4.3 and

ATOMDB version 1.3.1). The only exception is that the charge transfer inefficiency can not be corrected for all the Cas A data since they are acquired in GRADED mode. Fig. 1 shows the X-ray images of the four SNRs. Since the Cr line is very weak, we extracted the spectrum of each SNR from almost the entire source region, as illustrated in Fig. 1. The background spectra were extracted from the off-source regions.

Cas A and Kepler have been observed for a few times spanning 4 to 5 months. We therefore carefully performed the analysis to eliminate the effect of any CCD performance evolution with time. Taking Cas A as an example, we first created source and background spectra as well as the corresponding RMF and ARF files for each of the 9 observations (including IDs 4634, 4635, 4636, 4637, 4638, 4639, 5196, 5319, 5320), and then combined them with FTOOLS<sup>1</sup>. This process has taken into account the degradation of the CCD performance during the observation span. We noticed that there is no clear difference between the 9 RMF files, therefore the ARF files can be added with FTOOLS *addarf*. The total photon number of each source spectrum was taken as the corresponding adding weight. We performed a joint fit to the spectra of all the observations by using their respective RMF and ARF files, and found that the fitting results are consistent with those obtained by using the combined data and the added RMF and ARF. This demonstrates that the combining process works well and suggests that the gain is properly calibrated from observation to observation. The spectral fitting was done with XSPEC version 11.3.2 (Arnaud 1996).

The 0.5–8.0 keV spectra of the four SNRs are plotted in Fig. 2. Apparently the spectrum of Cas A has the best statistics, therefore we take it as an example to describe our spectral analysis process. We first fitted the continuum-dominant 4.2–6.0 keV spectrum with bremsstrahlung and power law models respectively. In both cases, three line-like features appear in the residual distribution. In this case, we added three Gaussian components to account for these lines. The fitting models and residuals are plotted in Fig. 3. The best fit centroid energies of the three lines are 4.607, 4.878 and 5.635 keV respectively. The power law model can represent the continuum emission better than the bremsstrahlung one, with  $\chi^2$  452.9 vs. 560.3 for 111 degrees of freedom (d.o.f.), although neither of the two fits is statistically acceptable. However, adapting different continuum models does not change the best fit results of the line strength significantly, e.g. the equivalent width (EW) of the 5.635 keV line is  $9.6 \pm 0.87$  eV with the power law model and  $10.7 \pm 0.95$  eV with the bremsstrahlung. For the other three SNRs, the power law model also fits the continuum emission better than the bremsstrahlung model does. The latter model seems to overestimate the spectra at low energies, while underestimating at high energies. In this case, the power law model was used

---

<sup>1</sup><http://heasarc.gsfc.nasa.gov/docs/software/ftools/>

in the following fitting process to account for the continuum emission. We also note here that the 4.2–6.0 keV spectrum of Cas A is more complicated than the model we used. This will be further discussed in § 3.2.

According to the Astrophysical Plasma Emission Code (APEC<sup>2</sup>), the two lines below 5.0 keV could be the He-like Ca-K emission, while the Ti-K emission could not be ruled out as it also emits around those energies. Unfortunately, Ti has not been considered in the currently available plasma codes, thus we cannot get the emissivities of the Ti lines to judge whether they represent these observed line features or not. Since the main topic of the current paper is Cr emission and the line candidates below 5.0 keV are beyond its scope, we only adopt data above 5.0 keV for the analyses of the continuum and line emission. As an element of the Fe-group, Cr is closely related to Fe in its synthesis process (Woosley & Weaver 1994; Woosley & Weaver 1995; Thielemann et al. 1996). A comparative study of the Fe and Cr emission should be important. Therefore we take the 5.0–7.5 keV spectra to study both the Cr and the Fe K lines in the following.

We note here that the systematic errors of the EWs and fluxes induced by using different continuum models and different energy ranges are included in the parameters’ confidence ranges in Tables 2 & 3. By fitting the 5.0–7.5 keV spectra of the four SNRs with bremsstrahlung to represent the continuum model, we can get the best fit EWs and fluxes of the Cr and Fe emission lines along with their 90% statistical errors. Likewise, by fitting these spectra with the continuum energy extended down to 4.2 keV, we can also get another set of best fit EWs, fluxes and their confidence ranges. The final confidence ranges listed in Tables 2 & 3 cover those from the above two fittings and from fitting with a power law continuum model to the data in 5.0–7.5 keV.

### 3. Results

#### 3.1. W49B

In the analysis of the *ASCA* spectrum, Hwang et al. (2000a) found evidence of the He-like Cr and Mn lines near 5.69 and 6.18 keV, and the existence of these lines was confirmed by *XMM-Newton* (Miceli et al. 2006). From the spectra (Fig. 2 (top left) and Fig. 4 (top left)), we can see that the Cr and Mn lines are also detected with *Chandra*. We fitted the 5.0–7.5 keV spectrum with a power law model plus three Gaussian components to account for the continuum, Cr, Mn and Fe lines respectively. Eliminating the Gaussian component

---

<sup>2</sup><http://xc.harvard.edu/atomdb>

for Cr (or Mn) leads to an increasing of  $\chi^2$ , from 93.4 for d.o.f 68 to 185.8 (or 103.7) for d.o.f 71. The Cr line emission is firmly detected in the *Chandra* spectrum, while the Mn line is less significant.

Fig. 4 (top left) shows the fitting model and residuals, and Table 2 gives the best fit results for the Cr and Fe lines, including line center energies and fluxes along with their uncertainties. The EWs of the two lines, calculated from the XSPEC command *eqwidth*, are given in the same table. From our fitting analyses, the Cr line center energy is  $E_{Cr} = 5.656^{+0.014}_{-0.016}$  keV, and the flux is  $f_{Cr} = (0.32^{+0.08}_{-0.07}) \times 10^{-4}$  photons  $\text{cm}^{-2} \text{s}^{-1}$ , while for the Mn line,  $E_{Mn} = 6.126^{+0.035}_{-0.030}$  keV and  $f_{Mn} = (0.10 \pm 0.05) \times 10^{-4}$  photons  $\text{cm}^{-2} \text{s}^{-1}$ . The fitted line parameters are generally in good agreement with those from *ASCA* and *XMM-Newton* (c.f Table 3).

### 3.2. Cas A

The 5.0–7.5 keV spectrum of Cas A is shown in Fig. 4 (top right). It was fitted with a power law (for continuum) plus three Gaussian components (for the lines). Two Gaussian components were used to represent the Fe-K complex since it cannot be well fitted by a single Gaussian profile. The centroid energies for these two Gaussian components are  $6.600 \pm 0.001$  keV and  $6.659 \pm 0.001$  keV, with their widths  $100 \pm 2$  eV and  $72 \pm 7$  eV respectively. The centroid energy of the Fe-K complex listed in Table 2 is the emission measure weighted mean value, while the flux and EW are the sums of the two components. The third Gaussian component is for the 5.635 keV line mentioned in § 2. Adding the third Gaussian leads to a much better fit (c.f. Fig. 3), with the reduced  $\chi^2$  decreasing from 993.8/65 to 222.9/62 for data in 5.0–6.0 keV. This represents a significant detection of the Cr-K line emission, and its best fit parameters are listed in Table 2 as well.

The requirement of two Gaussian components for the Fe-K complex is probably due to the Doppler shift variation across the whole remnant. Spatially resolved X-ray spectroscopy of Cas A by both *XMM-Newton* (Willingale et al. 2002) and *Chandra* (Yang et al. 2008) shows that different parts of this remnant are moving with different line of sight velocities, with typical value of  $\pm 1000$   $\text{km s}^{-1}$ . Considering this, we selected two regions based on the Doppler shift map from the *XMM-Newton* observation (Willingale et al. 2002), as illustrated in Fig.1. The spectra of the two regions are given in Fig. 5. They were fitted with a power law plus two Gaussian components, representing the continuum, Cr and Fe-K line emission. The Cr line is very significant in both spectra. Adding a Gaussian component for Cr leads to the reduced  $\chi^2$  decreasing from 440.0/62 to 197.4/59 and from 670.9/62 to 184.2/59 for the blueshifted and redshifted regions respectively in 5.0–6.0 keV. The fitted line center

energies of the Fe-K lines are  $6.591 \pm 0.001$  keV and  $6.669 \pm 0.001$  keV, which are generally consistent with the line center energies of the two components fitted to the Fe-K line of the whole remnant spectrum. This demonstrates that the Doppler shift dominates the structure of the Fe-K complex of Cas A. The centroid energies of the Cr line in the two regions are  $5.590^{+0.008}_{-0.007}$  and  $5.657^{+0.010}_{-0.008}$  keV, with a separation similar to that of the two Fe-K lines. The Cr and Fe ejecta are thus probably moving with similar velocity. We noticed that the Fe-K line from a small region of Cas A also cannot be well represented by one Gaussian component (c.f Fig. 5, residual distribution), suggesting small velocity difference even within such a scale (c.f Fig. 7 in Willingale et al. 2002).

On the other hand, the existence of more than one strong Fe-K line that cannot be resolved with *Chandra* ACIS could also contribute to the broadening of the Fe-K line in Cas A. Various Fe-K lines around this energy have been clearly displayed in the spectra of the cataclysmic variables V1223 Sagittarii (Mukai et al. 2001) and U Geminorum (Szkody et al. 2002) using data collected by the High Energy Transmission Grating onboard *Chandra*. The centroid energy difference of the two Gaussian components in Cas A is about 60 eV, which is comparable with the difference of the He-like triplet of Fe-K lines ( $\sim 65$  eV<sup>3</sup>). Higher energy resolution spectra from future missions will help us to resolve the Fe-K complex.

### 3.3. Tycho & Kepler

The 5.0–7.5 keV spectra of Tycho and Kepler are shown in Fig. 4. We first fitted the spectrum of Tycho with a power law (for continuum emission) plus one Gaussian component (for the Fe-K line). A line-like structure came out around 5.45 keV in the residual distribution. As the neutral Cr K line is near 5.4 keV while the H-like Cr K line is around 5.9 keV (c.f Table 4), this structure might be the Cr line in relatively low ionization state. In this case, we added a Gaussian component there, and the reduced  $\chi^2$  decreased from 36.6/21 to 11.4/18 in 5.0–6.0 keV. For the Kepler spectrum in the same energy range, adding a Gaussian component around 5.46 keV also leads to a reduction of the reduced  $\chi^2$  from 47.6/24 to 27.8/21. Finally, the 5.0–7.5 keV spectra of Tycho and Kepler were fitted with a power law (for continuum) plus two Gaussian components (one for the Cr line and the other for the Fe line). The fitting models and residual distribution are also given in Fig. 4.

The best fit parameters for the Cr and Fe lines are listed in Table 2, along with their confidence ranges. Although there are big uncertainties in the EWs and fluxes of Cr lines in both Tycho and Kepler, the detection of these lines is significant, judging from the changes

---

<sup>3</sup>c.f Mewe et al. 1985; [http://www.camdb.ac.cn/e/spectra/spectra\\_search.asp](http://www.camdb.ac.cn/e/spectra/spectra_search.asp)

of  $\chi^2$  mentioned above and the lower limits of the confidence ranges. From Table 2, we can see that the centroid energies of the putative Cr lines in Tycho and Kepler are about 200 eV lower than those of W49B and Cas A. This will be further discussed in § 4.1.

## 4. Discussion

### 4.1. The ionization state and spatial correlations between Cr and Fe

The different line center energies of the Cr emission lines in these SNRs reflects that the ionization states of Cr in these SNRs are dissimilar. The Cr in W49B is in relatively high ionization state since its line center energy is  $5.656_{-0.016}^{+0.014}$  keV (c.f Table 2). For Cas A, the centroid energy of the Cr line is  $5.635_{-0.005}^{+0.007}$  keV, which also suggests a high ionization state of Cr. The center energies of the putative Cr lines in Tycho and Kepler are about 200 eV lower than those in W49B and Cas A. If these lines do come from Cr, it should be in a relatively low ionization state (c.f Table 4). We noticed that the Fe-K line center energies in Tycho and Kepler are both around 6.44 keV. This implies low ionization states of Fe as well, as suggested by previous observations (Tsunemi et al. 1986; Hwang et al. 1998; Hwang et al. 2002; Kinugasa & Tsunemi 1999).

In Fig. 6, we plot the Cr line center energy versus that of the Fe line in these four SNRs. The theoretical centroid energies of Cr and Fe K lines in different ionization states given in Table 4 are overplotted in the same figure. Obviously, there is a positive correlation between the two line center energies both theoretically and observationally. We can conclude from Fig. 6 that the emission lines around 5.46 keV in Tycho and Kepler are from Cr. Meanwhile, the Cr in Cas A and W49B might be He/Li-like, while Ne-like or an even lower ionization state in Tycho and Kepler. Since the line center energy is closely related to the ionization ages of the emitting plasma, such a positive correlation implies that the ionization ages of Cr and Fe are closely related to each other.

The above ionization state correlation suggests that the Cr and Fe ejecta are co-located, which is also supported by the spectra of the blueshift and redshift regions in Cas A. As shown in § 3.2, the Cr and Fe ejecta are probably moving with the same velocity as implied by the centroid energies of the Cr and Fe lines from these two regions. Meanwhile, the EW ratio of the Cr line to the Fe line in the blueshift region spectrum is 0.82%, while it is 0.91% in the redshift one. They are both consistent with the overall value ( $0.85_{-0.07}^{+0.18}\%$ , c.f. Table 2) within the confidence range. This is further evidence that Cr and Fe are co-located.

According to the nucleosynthesis theory (Woosley & Weaver 1994; Woosley et al. 1995),  $^{50}\text{Cr}$  is generated by explosive oxygen and silicon burning, while  $^{52,53}\text{Cr}$  are the products of

$^{52,53}\text{Fe}$  decay in explosive silicon burning. The most abundant Fe is  $^{56}\text{Fe}$  decayed from  $^{56}\text{Ni}$ , which is also produced mainly from explosive silicon burning. Among all the isotopes of Cr,  $^{52}\text{Cr}$  is the most abundant, and its production is generally at least one order of magnitude greater than the others (Nomoto et al. 1984; Woosley et al. 1995). In this case, most of the Cr would be located near and thus share a similar ionization time with Fe in SNRs. Cayrel et al. (2004) observed a number of so-called “first stars”, i.e. very metal-poor dwarfs and giants. They found that the scatter of the Cr/Fe values of these stars is very small, indicating that the production of Fe and Cr are very closely linked. Our results are consistent with the theoretical predictions and further strengthen the previous observational statement in a different way.

#### 4.2. Using the Cr to Fe EW ratio to constrain the SN explosion process

Many theoretical calculations of nucleosynthesis have included Cr for both Ia (Woosley & Weaver 1994; Iwamoto et al. 1999) and core-collapse SNe (Woosley & Weaver 1995; Thielemann et al. 1996; Maeda & Nomoto 2003). In order to compare with these models, we need the mass (or abundance) ratio between Cr and the other elements. Hwang et al. (2000a) interpolated the  $\text{He}\alpha$  emissivity of Cr from those of Si, S, Ar, Ca and Fe, using the Raymond-Smith (RS) code for the 2 keV plasma in collisional ionization equilibrium (CIE), and then calculated the Cr abundance of W49B. They found that the Cr and Fe abundances are consistent with a solar ratio, corresponding to an atomic number ratio 1.0% of Cr to Fe (Anders & Grevesse 1989) and thus a mass ratio  $M_{\text{Cr}/\text{Fe}} \sim 0.9\%$ . Cr and Fe in Tycho and Kepler are in relatively low ionization state, and as emissivities in these states are not well calculated for elements such as Si, S, Ar, Ca, and Fe, it is difficult to interpolate the Cr emissivity as done by Hwang et al. (2000a). However, according to the discussion in §4.1, Cr and Fe are spatially correlated and thus have similar temperatures and ionization ages, therefore the EW ratio of the Cr and Fe K lines ( $\text{EW}_{\text{Cr}/\text{Fe}}$ ) would be a good representation of the mass ratio of these two elements. Considering this, we use the EW ratio for the discussion below.

From Table 2, we can see that  $\text{EW}_{\text{Cr}/\text{Fe}}$  of these four SNRs differ from one another. This ratio might be used to constrain the properties of the corresponding SNe. Badenes et al. (2006) have made detailed comparisons of the X-ray spectra of the type Ia SNR Tycho with the theoretical models. They found the one-dimensional delayed detonation model can well reproduce its X-ray emission. From numerical calculations, the standard SNe Ia models, i.e carbon deflagration and Chandrasekar mass models (e.g W7, W70 etc, Nomoto et al. 1984) often yield relatively small  $M_{\text{Cr}/\text{Fe}}$  ( $< 1\%$ , Nomoto et al. 1997; Iwamoto et al. 1999).



Multi-dimension models based on W7 also give similar  $M_{Cr/Fe}$  (Travaglio et al. 2004; 2005). On the other hand, the delayed detonation models (WDD, CDD etc) produce much larger  $M_{Cr/Fe}$  ( $> 2\%$ ), and  $M_{Cr/Fe}$  decreases as the transition density increases (Nomoto et al. 1997; Iwamoto et al. 1999). Therefore, our observational results of Tycho suggest that there should be a deflagration-detonation transition at some stage of Tycho’s SN explosion, which further confirm the results of Badenes et al. (2006). Meanwhile, we favor a relatively small transition density, probably  $1.7 \times 10^7 \text{ g cm}^{-3}$  (Nomoto et al. 1997; Iwamoto et al. 1999). This is also consistent with that suggested by Badenes et al. (2006,  $2.2 \times 10^7 \text{ g cm}^{-3}$ ).

Cas A has been identified as the remnant of a core-collapse SN. The recent study of its progenitor implies the mass to be 15–25  $M_{\odot}$  (Young et al. 2006). According to the calculations of spherical models by Thielemann et al. (1996), a  $20M_{\odot}$  progenitor gives a  $M_{Cr/Fe}$  of 1.2%, which is higher than our measured value. However the non-spherical explosion may lead to a smaller  $M_{Cr/Fe}$  (Maeda & Nomoto 2003). It has already been suggested that the explosion of Cas A is asymmetric, based on the jet structure (Hwang et al. 2004) and the Doppler map (Willingale et al. 2002). Meanwhile, a bigger progenitor mass would lead to a smaller mass cut and thus smaller  $M_{Cr/Fe}$ , since Cr is mainly produced in the incomplete Si-burning zone (Umeda & Nomoto 2002). Therefore, we support a higher progenitor mass (Young et al. 2006) and the asymmetric explosion scenario for Cas A.

The classifications of W49B and Kepler are not conclusive. For W49B, Hwang et al. (2000a) compared the relative abundances of Mg, S, Ar, Ca, Fe and Ni to Si, and suggested that W49B may have a type Ia progenitor. However they claimed that a low mass (13–15  $M_{\odot}$ ) type II progenitor is also possible. The *Chandra* image of W49B shows a bipolar jet, which was taken as evidence for a gamma-ray burst (GRB) remnant<sup>4</sup>. This was further supported by multi-band observations (Keohane et al. 2007). The nucleosynthesis calculation for bipolar core-collapse SN explosions (Maeda & Nomoto 2003) generally predicts an  $EW_{Cr/Fe}$  of  $1.0 \pm 0.5\%$ , which matches the observations perfectly (Hwang et al. 2000a; Miceli et al. 2006; this paper). Kepler tends to be identified as a type Ia SNR (Reynolds et al. 2007). If so, the small  $EW_{Cr/Fe}$  would favor the carbon deflagration models (W7, W70 etc) rather than those involving detonation (Nomoto et al. 1997; Iwamoto et al. 1999; Travaglio et al. 2004; 2005).

The above discussions are based on the overall mass ratio of Cr to Fe in an SNR. It is possible that in these SNRs there are still a fraction of Fe and Cr that has not been overtaken by the reverse shock and so invisible in X-rays. However, according to our discussion in §4.1, Cr and Fe should be well mixed, so the observed EW ratio of Cr to Fe could represent the

---

<sup>4</sup>[Http://chandra.harvard.edu/press/04\\_releases/press\\_060204.html](http://chandra.harvard.edu/press/04_releases/press_060204.html)

overall Cr to Fe mass properly. Therefore the main conclusions are reliable no matter what fraction of Fe is observed.

## 5. Summary

We performed a Cr K line survey with the *Chandra* data in young SNRs W49B, Cas A, Tycho and W49B. We confirmed the Cr line in W49B, and gave a consistent flux and line center energy with respect to the previous results. Then we report, for the first time, the detection of Cr lines in Cas A, Tycho and Kepler. We conclude that Cr in Cas A is in a high ionization state similar to that of W49B, while Cr is in a low ionization state low in Tycho and Kepler. We find that Cr and Fe have similar ionization states and are co-located in these four SNRs. The reason might be that Cr and Fe are synthesized by the same process deep inside the progenitor. We propose that the EW ratio of Cr to Fe might be used as an supplementary constraint on the properties of the SN explosions. For the type Ia SNR Tycho,  $EW_{Cr/Fe}$  favors the delayed detonation model with relatively small transition density ( $1.7 \times 10^7 \text{ g cm}^{-3}$ ) from deflagration to detonation. This is consistent with the model suggested by Badenes et al. (2006) from the comparison of Tycho's X-ray spectra with theoretical calculations. The relatively small  $EW_{Cr/Fe}$  in Cas A and W49B suggests their asymmetric explosions, which is also consistent with the previous results. If we adopt the type Ia origin for Kepler, its small  $EW_{Cr/Fe}$  could be attributed to the carbon deflagration explosion.

We are grateful to the anonymous referee for very helpful comments and suggestions leading to significant improvements of the paper. The manuscript is read by Dr. E. Miller in MIT. This work is supported by the Nature Science Foundation of China through grants 10533020, 10573017, 10778716 and by a Grant-in-Aid for Scientific Research by the Ministry of Education, Culture, Sports, Science and Technology, Japan(16002004).

## REFERENCES

- Anders, L., & Grevesse, N. 1989, *Geochim. Cosmochim. Acta*, 53, 197
- Arnaud, K. A. 1996, *ASPC*, 101, 17
- Badenes, C., Borkowski, K. J., Hughes, J. P., Hwang, U., & Bravo, E. 2006, *ApJ*, 645, 1373

- Cassam-Chenaï, G., Decourchelle, A., Ballet, J., Hwang, U., Hughes, J. P., Petre, R. 2004, *A&A*, 414, 545
- Cayrel, R., Depagne, E., Spite, M., Hill, V., Spite, F., Francois, P., Plez, B., Beers, T., Primas, F., Andersen, J., et al. 2004, *A&A*, 416, 1117
- Hatsukade, I., Tsunemi, H., Yamashita, K., Koyama, K., Asaoka, Y., & Asaoka, I. 1990, *PASJ*, 42, 279
- Holt, S. S., Gotthelf, E. V., Tsunemi, H., & Negoro, H. 1994, *PASJ*, 46, L151
- Hwang, U., Decourchelle, A., Holt, S. S., Petre, R. 2002, *ApJ*, 581, 1101
- Hwang, U., & Gotthelf, E. V. 1997, *ApJ*, 475, 665
- Hwang, U., Hughes, J. P., Petre, R. 1998, *ApJ*, 497, 833
- Hwang, U., Laming, J. M., Badenes, C., et al. 2004, *ApJ*, 615, L117
- Hwang, U., Petre, R., Hughes, J. P. 2000a, *ApJ*, 532, 970
- Hwang, U., Holt, S. S., & Petre, R. 2000b, *ApJ*, 537, L119
- Hughes, J. P., Hayashi, I., Helfand, D., Hwang, U., Itoh, M., Kirshner, R., Koyama, K., Markert, T., Tsunemi, H., & Woo, J. 1995, *ApJ*, 444, L81
- Hughes, J. P., Rakowski, C. E., Burrows, D. N., & Slane, P. O. 2000, *ApJ*, 528, L109
- Iwamoto, K., Brachwitz, F., Nomoto, K., Kishimoto, N., Umeda, H., Hix, W. R., & Thielemann, F-K 1999, *ApJS*, 125, 439
- Keohane, J. W., Reach, W. T., Rho, J., & Jarrett, T. H. 2007, *ApJ*, 654, 938
- Kinugasa, K., & Tsunemi, H. 1999, *PASJ*, 51, 239
- Maeda, K. & Nomoto, K. 2003, *ApJ*, 598, 1163
- Mewe, R., Gronenschild, E. H. B. M. & van den Oord, G. H. J. 1985, *A&A*, 62, 197
- Mukai, K., Kallman, T., Schlegel, E., Bruch, A., Handler, G. & Kemp, J. 2001, *ASPC*, 251, 90
- Miceli, M., Decourchelle, A., Ballet, J., Bocchino, F., Hughes, J. P., Hwang, U., & Petre, R. 2006, *A&A*, 453, 567

- Nomoto, K., Thielemann, F.K., & Yokoi, K. 1984, ApJ, 286, 644
- Nomoto, K., Iwamoto, K., Nakasato, N., Thielemann, F.-K., Brachwitz, F., Tsujimoto, T., Kubo, Y., & Kishimoto, N. 1997, NuPhA, 621, 467
- Rakowski, C. E., Badenes, C., Gaensler, B. M., Gelfand, J. D., Hughes, J. P. & Slane, P. O. 2006, ApJ, 646, 982
- Reynolds, S. P., Borkowski, K. J., Hwang, U., Hughes, J. P., Badenes, C., Laming, J. M., & Blondin, J. M. 2007, ApJ, 668, L135
- Szkody, P., Nishikida, K., Raymond, J. C., Seth, A., Hoard, D. W., Long, K. S., & Sion, E. M. 2002, ApJ, 574, 942
- Thielemann, F.-K, Nomoto, K., & Hashimoto, M. 1996, ApJ, 460, 408
- Travaglio, C., Hillebrandt, W., Reinecke, M., & Thielemann, F.-K. 2004, A&A, 425, 1029
- Travaglio, C., Hillebrandt, W., & Reinecke, M. 2005, A&A, 443, 1007
- Tsunemi, H., Yamashita, K., Masai, K., Hayakawa, S., & Koyama, K. 1986, ApJ, 306, 248
- Umeda, H., & Nomoto, K. 2002, ApJ, 565, 385
- Willingale, R., Bleeker, J. A. M., van der Heyden, K. J., Kaastra, J. S., & Vink, J. 2002, A&A, 381, 1039
- Woosley, S. E., & Weaver, T. A. 1994, ApJ, 423, 371
- Woosley, S. E., Langer, N., & Weaver, T. A. 1995, ApJ, 448, 315
- Woosley, S. E., & Weaver, T. A. 1995, ApJS, 101, 181
- Yang, X.J., Lu, F.J., & Chen, L. 2008, ChJAA, 8, 439
- Young, P. A., Fryer, C. L., Hungerford, A., Arnett, D., Rockefeller, G., Timmes, F. X., Voit, B., Meakin, C., Eriksen, K. A. 2006, ApJ, 640, 891

Table 1: Information of *Chandra* observations we used

Target	Obs_ID	$t_{exp}(ks)$	Obs-date
W49B	117	~50	July, 2000
Cas A	VLP*	~1000	February~May, 2004
Tycho	115	~50	September, 2000
Kepler	LP†	~750	April~August, 2006

\*Very Large Project, Observation IDs: 4634, 4635, 4636, 4637, 4638, 4639, 5196, 5319 and 5320.

†arge Project, Observation IDs: 6714, 6715, 6716, 6717 and 6718.

Table 2: The Cr and Fe line parameters of W49B, Cas A, Tycho and Kepler

SNR	Cr			Fe			$EW_{Cr/Fe}$
	line center eV	EW eV	flux $\frac{10^{-4}photons}{cm^2s}$	line center eV	EW eV	flux $\frac{10^{-4}photons}{cm^2s}$	
W49B	$5656^{+14}_{-16}$	$79.6^{+20.3}_{-18.2}$	$0.32^{+0.08}_{-0.07}$	$6666^{+1}_{-2}$	$5000^{+280}_{-250}$	$10.2^{+0.6}_{-0.5}$	$1.6^{+0.40\%}_{-0.36\%}$
CasA	$5635^{+7}_{-5}$	$8.31^{+1.72}_{-0.69}$	$0.65^{+0.13}_{-0.05}$	$6633^{+1}_{-1}$	$981^{+12}_{-10}$	$48.3^{+0.03}_{-0.03}$	$0.85^{+0.18\%}_{-0.07\%}$
Tycho	$5465^{+45}_{-50}$	$46.2^{+40.8}_{-14.6}$	$0.33^{+0.29}_{-0.10}$	$6436^{+6}_{-7}$	$1280^{+52}_{-42}$	$6.13^{+0.24}_{-0.22}$	$3.6^{+3.2\%}_{-1.1\%}$
Kepler	$5469^{+40}_{-45}$	$16.5^{+8.0}_{-6.6}$	$0.03^{+0.014}_{-0.012}$	$6443^{+1}_{-2}$	$2630^{+80}_{-30}$	$3.61^{+0.05}_{-0.04}$	$0.63^{+0.30\%}_{-0.25\%}$

Table 3: The Cr, Mn and Fe line parameters of W49B from different instruments.

Instrument	Cr		Mn		Fe	
	line center eV	flux $\frac{10^{-4}photons}{cm^2s}$	line center eV	flux $\frac{10^{-4}photons}{cm^2s}$	line center eV	flux $\frac{10^{-4}photons}{cm^2s}$
<i>ASCA</i> <sup>a</sup>	$5685^{+20}_{-27}$	$0.30^{+0.08}_{-0.11}$	$6172^{+47}_{-49}$	$0.13^{+0.14}_{-0.06}$	$6658^{+3}_{-2}$	$8.30 \pm 0.30$
<i>XMM-Newton</i> <sup>b</sup>	$5660 \pm 10$	$0.25 \pm 0.04$	$6170 \pm 50$	$0.10 \pm 0.03$	–	–
<i>Chandra</i> <sup>c</sup>	$5656^{+14}_{-16}$	$0.32^{+0.08}_{-0.07}$	$6126^{+35}_{-30}$	$0.10 \pm 0.05$	$6666^{+1}_{-2}$	$10.2^{+0.6}_{-0.5}$

<sup>a</sup>Hwang et al. 2000a

<sup>b</sup>Miceli et al. 2006

<sup>c</sup>this paper

Table 4: The K shell line energies of Cr and Fe in different ionization states.

element	neutral <sup>a</sup>	B-like <sup>b</sup>	Be-like <sup>b</sup>	Li-like <sup>b</sup>	He-like <sup>b</sup>	H-like <sup>c</sup>
Cr <sup>†</sup>	5.420	5.533	5.580	5.657	5.665	5.916
Fe <sup>‡</sup>	6.405	6.549	6.617	6.652	6.674	6.966

<sup>a</sup>K $\alpha$  line energy

<sup>b</sup>line energy with transition from level 2p to 1s

<sup>c</sup> $\gamma$  line energy

<sup>†</sup>[http://www.camdb.ac.cn/e/spectra/spectra\\_search.asp](http://www.camdb.ac.cn/e/spectra/spectra_search.asp)

<sup>‡</sup>Mewe et al. 1985

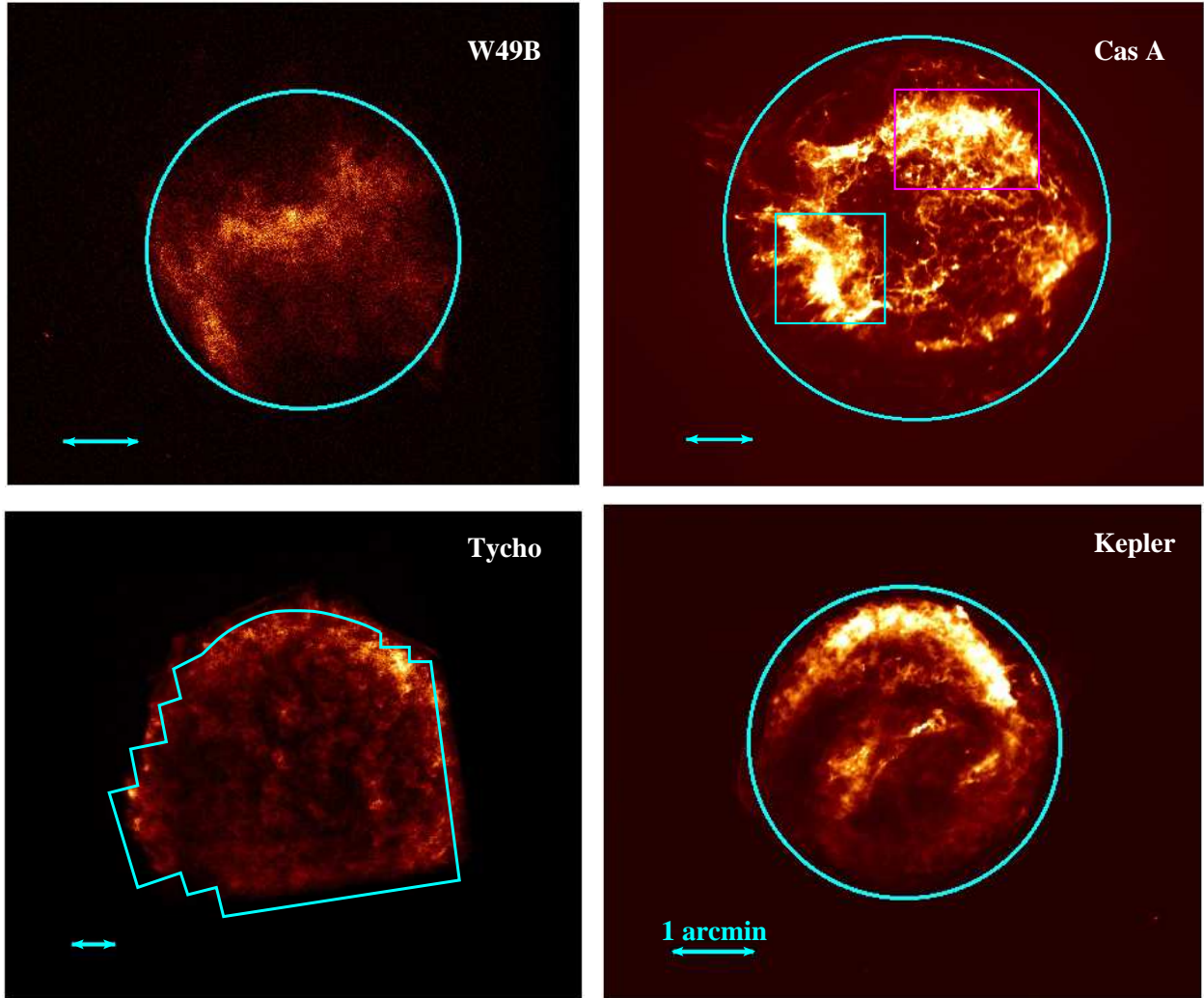


Fig. 1.— *Chandra* images of W49B, Cas A, Tycho and Kepler. The source spectral regions are overplotted. In order to cover the whole Tycho SNR, we use multi-regions as shown in the stretch. The double-arrwed lines represent 1 arcmin for the corresponding image. The two boxes in the Cas A image represent the blueshift (southeast, blue one) and redshift (northwest, red one) dominated portions we selected to create the spectra as described in § 3.2.

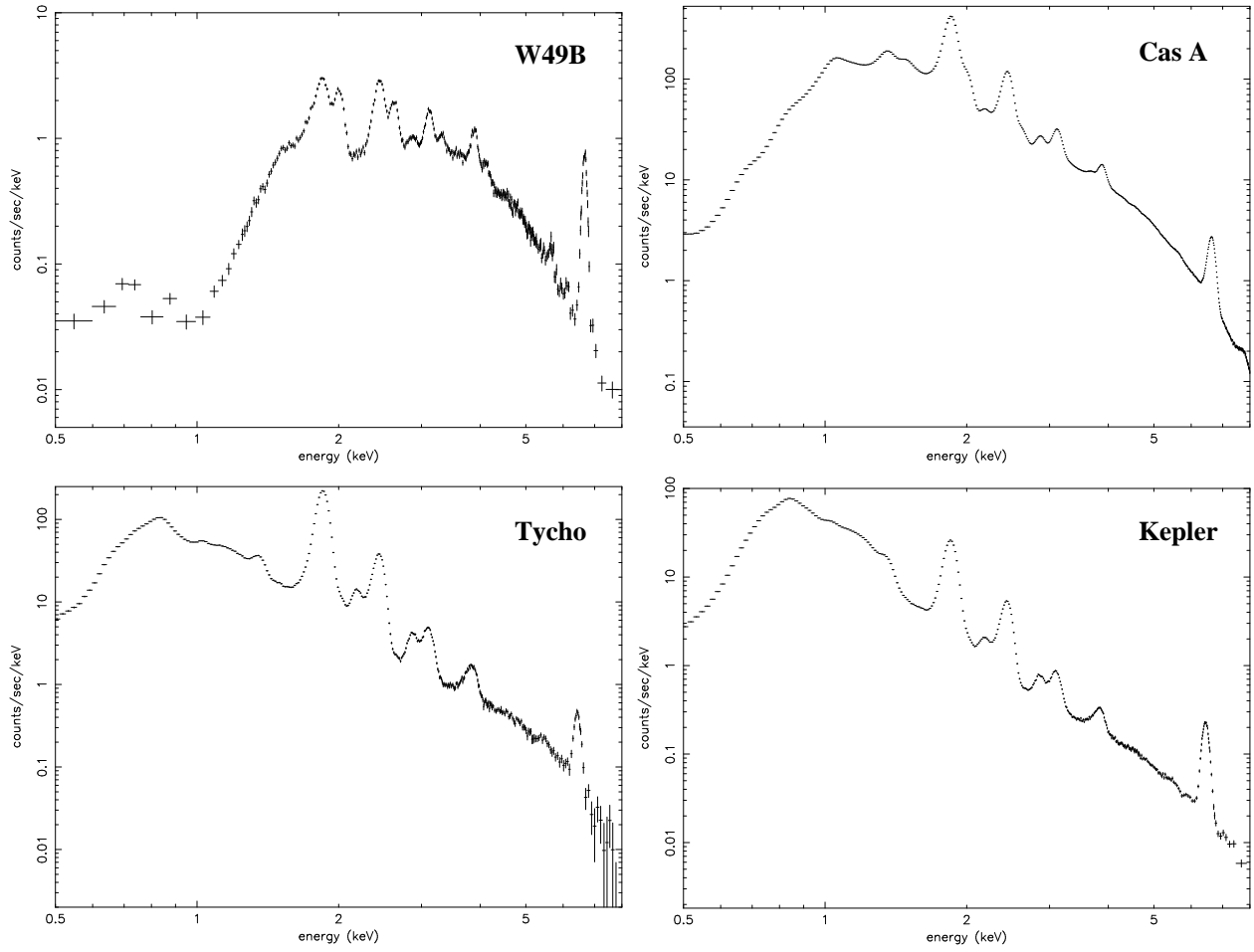


Fig. 2.— The 0.5–8.0 keV spectra of W49B, Cas A, Tycho and Kepler.



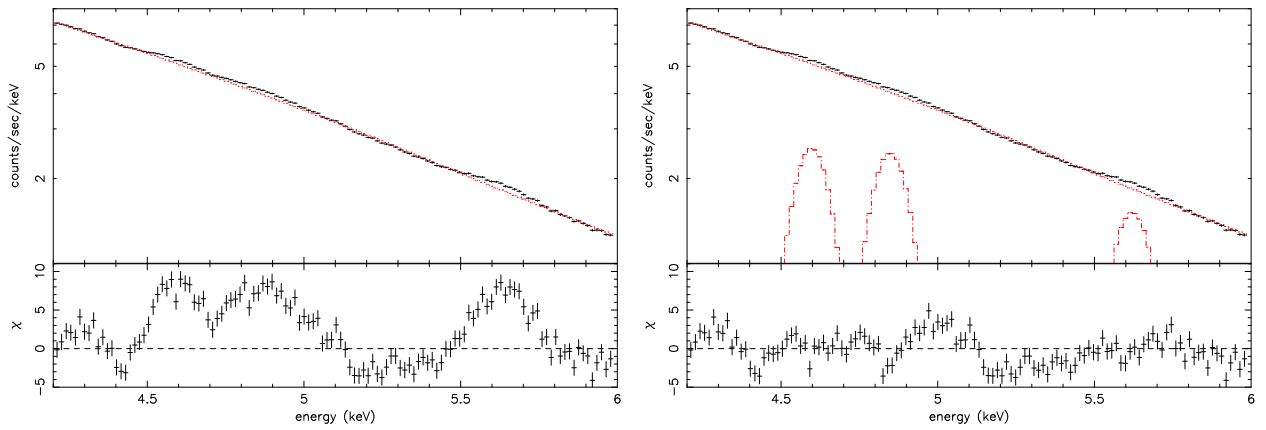


Fig. 3.— The 4.2–6.0 keV spectrum of Cas A fitting with different models. The left panel presents the fitting with one power law, while the right panel one power law plus three Gaussian components. The residual (normalized by sigma,  $\chi$ ) distributions are also plotted. The strength of all the Gaussian components are multiplied by a factor of 15, so as to be shown clearly.

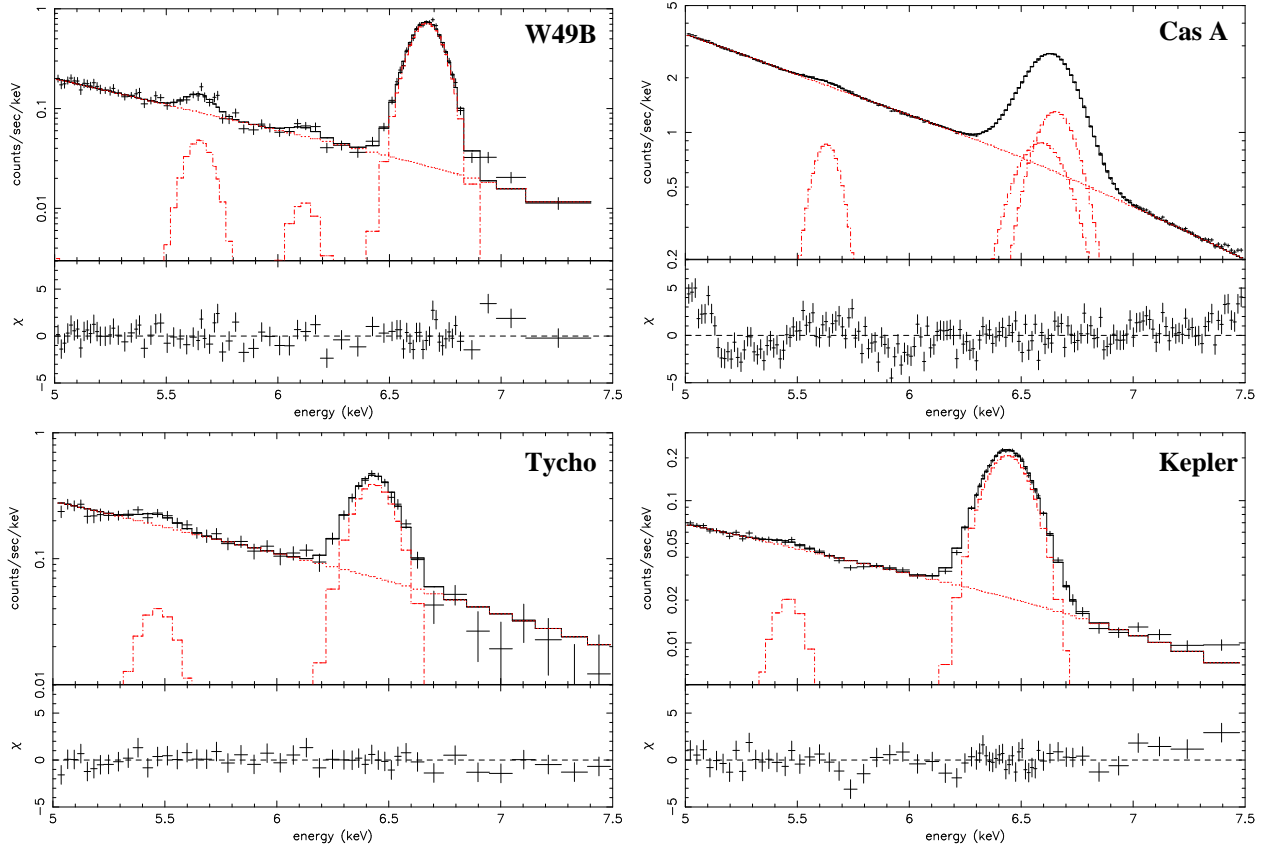


Fig. 4.— The 5.0–7.5 keV spectra of W49B, Cas A, Tycho and Kepler. The lines represent the fitting models as described in § 3. The strength of the Cr line for Cas A is multiplied by a factor of 10, while that for Kepler a factor of 5.

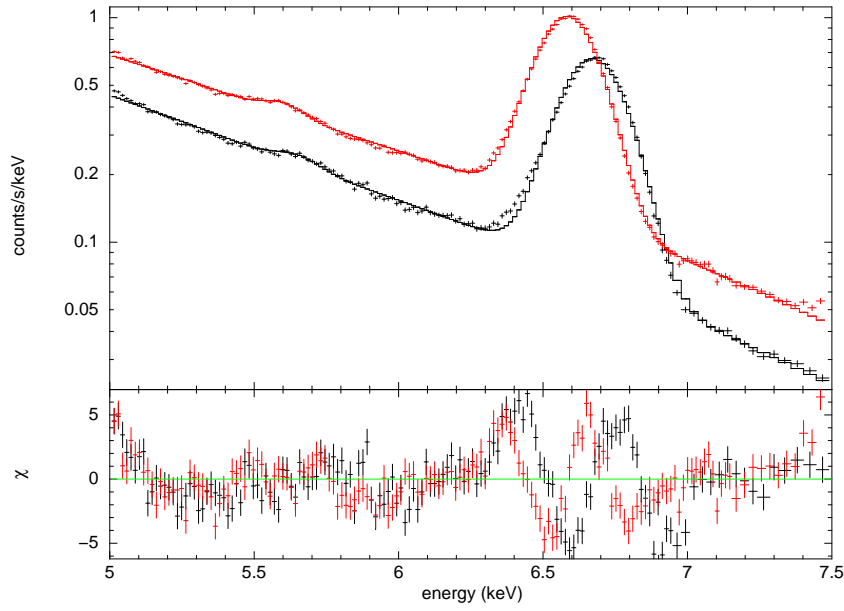


Fig. 5.— The 5.0–7.5 keV spectra of Cas A from the redshift (upper curve) and blueshift (lower curve) dominated portions. They are both fitted with a model involving a power law plus two Gaussian components.

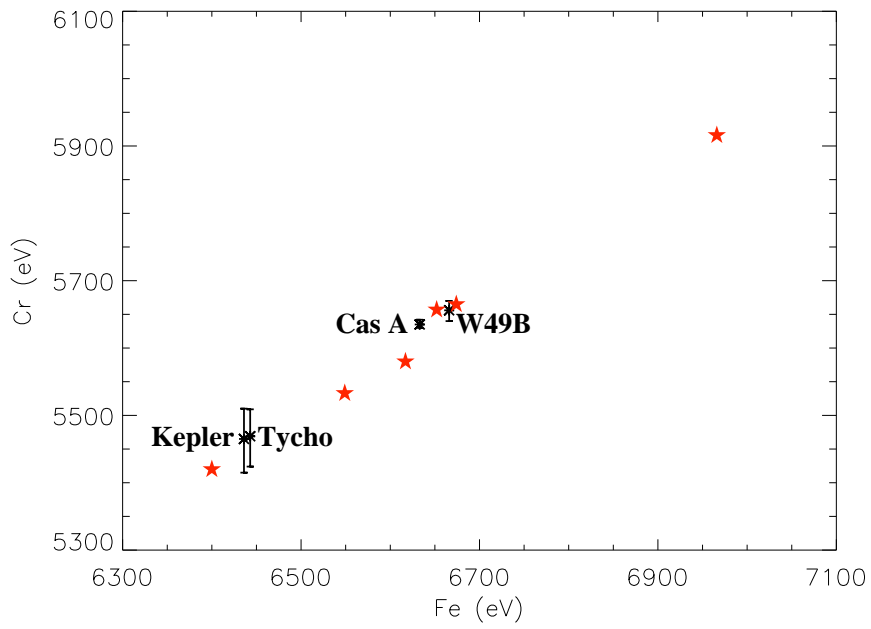


Fig. 6.— The line center energy of Cr versus Fe in W49B, CasA, Tycho and Kepler. The errors of the Fe line are not plotted, since they are almost within the size of the symbols. The stars represent the line center energy of Cr and Fe in various ionization states, as given in Table 4.